Detonation thermodynamic state statistics: 2D and 3D simulations in hydrogen-oxygen

Jackson Crane[1,*], Jonathan T. Lipkowicz[2], Xian Shi[3],
Irenaeus Wlokas[2], Andreas M. Kempf[2], Hai Wang[4]

[1]Department of Mechanical and Materials Engineering,
Queen's University, Kingston, ON Canada

[2]Chair of Fluid Dynamics, Faculty of Engineering,
University of Duisburg–Essen, Duisburg, Germany

[3]Department of Mechanical and Aerospace Engineering,
University of California, Irvine, Irvine, CA, USA

[4]Department of Mechanical Engineering, Stanford University, Stanford, CA, USA

1 Introduction

Developing modeling approaches for detonation propagation requires a detailed understanding of the thermodynamic states inherent to the phenomena. This is particularly relevant for non-linear physics such as finite-rate kinetics and non-equilibrium thermodynamics [1]. It is well understood that confinement plays a strong role on detonation structure [2–4]. The question we have in this work is whether the apparent differences in structure between different confinements manifests in substantially different thermodynamic states. Various statistical descriptions of detonation have been pursued, including describing mean structure via Favre-averaging [5], frontal velocity statistics [6], and cellular structure variability [7]. In this work we focus on describing temperature and pressure statistics to quantify the range and likelihood of various thermodynamic states in detonation structure. It may also provide an alternate framework to post-process detonation simulations. The simulations used to perform the statistical analysis include high-resolution 3D simulations of a square channel and a round tube, and a 2D simulation of a channel. The mixture considered is stoichiometric hydrogen-oxygen with 3000 PPMv of ozone additive, selected because it has been well-characterized experimentally [3, 7]. These simulations are described in our previous work [4], where detailed structural characterization is presented. We use this structural characterization to interpret the statistical results presented herein.

2 Numerical solver and setup

The simulations are performed with the in-house code *PsiPhi* [8, 9] that solves the fully compressible set of conservation equations for mass, momentum, total internal energy, and partial densities (Navier-Stokes) to simulate detonation wave propagation. The equations are discretized on an equidistant Cartesian grid utilizing the Finite Volume Method. An approximate Riemann solver computes convective fluxes at cell interfaces with the aid of a monotonicity preserving reconstruction scheme featuring a theoretical accuracy of 5th order, while a 2nd order central difference schemes is used for diffusive fluxes.

* Correspondence to: jackson.crane@queensu.ca

A Strang Operator Splitting framework allows explicit time integration of convection and diffusion with a 3rd order accurate Runge-Kutta scheme, while the implicit solver CVODE advances the solution in time from reaction. Sub-filter dynamics are modeled with an eddy viscosity/diffusivity approach, and the filtered chemical source term is modeled with a tophat PDF for temperature to account for non-linear reaction rate constants. More details can be found in [4, 8, 9].

The reaction kinetics are modeled with the Foundational Fuel Chemistry Model Version 1.0 (FFCM-1) [10, 11] with the Princeton ozone sub-model [12]. Two 3D geometries are considered: a square channel 12 x 12 x 12 mm, and a tube 12 mm in diameter and 12 mm in length, and one 2D geometry, 24 mm in width and 36 mm in length. The tube simulation is set up in a rectangular domain, where the effects of walls are modelled with the immersed boundary technique. The boundary conditions used are no-slip and isothermal (300 K) for the walls, a Dirichlet boundary condition for the inlet, and a partially reflecting boundary condition for the outlet. This setup allows the numerical domain to be moved at the average wave speed relative to the laboratory reference without wave reflection. The numerical resolution considered in all simulations is 10 µm. Detailed convergence information is included in [4].

3 Results

Reproduced from [4], Figure 1 presents isometric views of pressure snapshots from the 3D simulations. Clear differences are seen in macroscopic frontal structure between the 3D square channel (Fig. 1a) and the 3D round tube (Fig. 1b). The 3D square channel exhibits a square latticed frontal shock structure that contains 'line' blasts and 'point' blasts. Meanwhile, the 3D tube simulation contains varied blast structures that are statistically more distributed as compared to the 3D square channel. See [4] for more details, including quantitative analysis on the cell structure, blast dynamics and bulk propagation velocity.

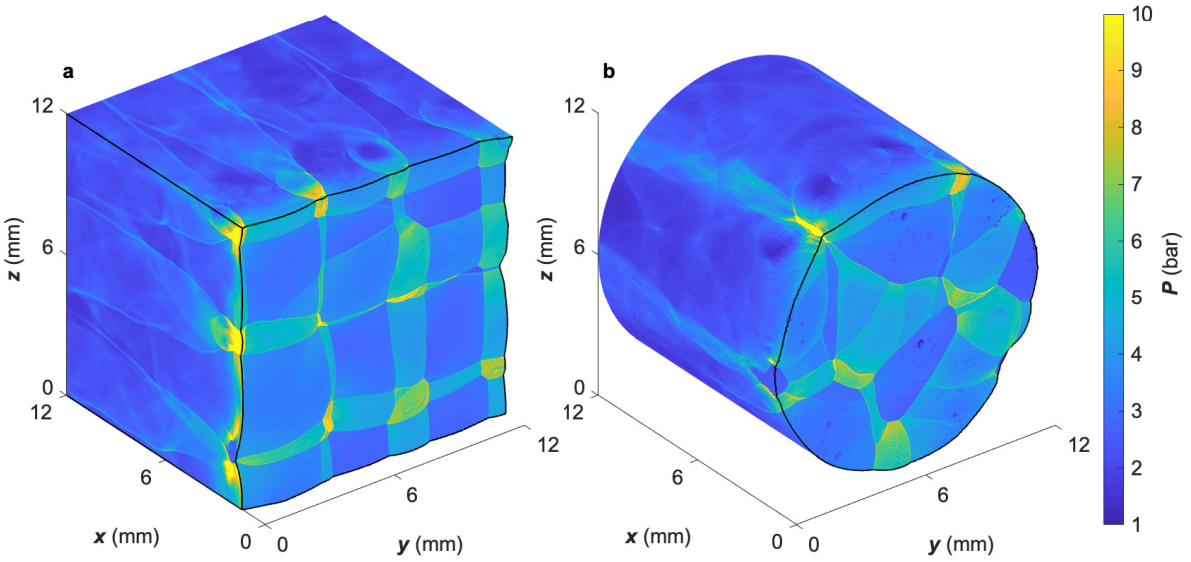

Figure 1: Isometric snapshots of the 3D square channel simulation (**a**) and the 3D round tube simulation (**b**) at the 20 µm grid resolution. Both are taken from the well-converged portions of the simulations. Plotted is pressure pseudocolor; the colorbar applies to both figures. Mixture and conditions of both simulations are stoichiometric hydrogen-oxygen with 3000 PPMv ozone additive at 15 kPa initial pressure. Reproduced from [4].

To analyze the statistical characteristics of the detonation, we first transform the stream-wise direction

(x) to distance behind the shock wave (x') for all values of y for 2D simulations and all values of y and z for 3D simulations. Figure 2 presents a set of 2D histograms, considering the probability density of temperature on the abscissa and pressure on the ordinate. The first three rows of Fig. 2 consider states from a single x' location (± 2 grid points $= 20$ μm). Included in these 2D histograms are $O(10^8)$ grid points for the 3D simulations and $O(10^7)$ grid points for the 2D simulation for the single x' location plots. The final row shows all post-shock grid points in the simulations ($O(10^{11})$ and $O(10^{10})$ points for the 3D and 2D simulations, respectively). We note that for the final row, a more physically relevant statistical subset is all points within the separatrix [13], but due to data storage limitations, the separatrix location is not available.

The thermodynamic states immediately behind the shock wave ($x' = 0.04$ mm, first row of Fig. 2) are concentrated within a narrow band of pressure and temperature. This is unsurprising: temperature and pressure are coupled for a shocked gas with frozen composition. The states lie on either side of the ZND solution (red dot) due to the cyclical nature of detonation cells (overdriven to underdriven). In both 3D simulations (square and tube) lower temperature/pressure conditions exist as compared to the 2D simulation, corresponding to slower shock speeds. It is postulated that the cause of the slower shocks in the 3D simulation is because the 3D confinement leads to faster shock decay (i.e., spherical vs. cylindrical blasts). In this x' location, little difference is observed between the square and round tube 3D simulations (first and second column).

Moving further away from the shock front, corresponding, on average, to the end of the induction length ($x' = 0.76$ mm, second row of Fig. 2), the set of thermodynamic states is substantially broader. At this location, a notable difference is observed between the 3D square and 3D tube simulations. The 3D square simulation presents a bimodal distribution of states, while the tube simulation presents a broader monomodal distribution. This is presumably due to the differences in structural characteristics observed in [4] and described briefly above. The difference between the 2D and 3D simulations is even more striking: the 2D simulation lies in several relatively narrow bands of states, while the 3D simulation distributions are more diffuse. 3D simulations exhibit a broader set of states because the blast dynamics are more variable in 3D: there exist 'line' blasts and 'point' blasts in 3D simulations, while 2D simulations only exhibit 'infinite line' blasts.

Towards the end of the reaction zone ($x' = 2.0$ mm, third row of Fig. 2) the two 3D simulations look more or less identical again. These states are at substantially higher temperatures and somewhat lower pressures as compared to those earlier in the profile, corresponding to burned gas. Again, the 3D solutions contain a broader set of states as compared to the 2D simulation.

The entire set of post-shock data is shown in the final row of Fig. 2 with the ZND solution (blue line) superimposed. Notable for all simulations is that the thermodynamic states found in the multi-dimensional simulation are much broader than those found in the ZND solution. The probability is highest for the burned gas region, where the bulk of the post-shock simulation lies, but is also pronounced for the post-shock region. The reaction region is somewhat less probable due to the short timescale associated with chemical reactions. Consistent with the single x' locations is that the 3D simulations contain a much broader and more diffuse set of states as compared to the 2D simulations, including somewhat higher and lower temperatures, and substantially higher and lower pressures.

The mean structure, as a function of x', is calculated by Reynolds-averaging across y for 2D simulations and across y and z for 3D simulations, as performed in [5]. The resultant temperature and pressure profiles for the 3 simulations is compared to the ZND simulation in Fig. 3. While the 3D square channel and 3D round tube exhibit qualitatively different frontal structure, and feature different cell sizes (5 mm in square channel vs. 7 mm in round tube, see [4]), their mean structure is nearly identical. The average velocity is also nearly identical between the two simulations (2,661 m/s for square channel vs. 2,656 m/s for round tube as compared to a CJ velocity of 2,734 m/s). These results suggest that even though

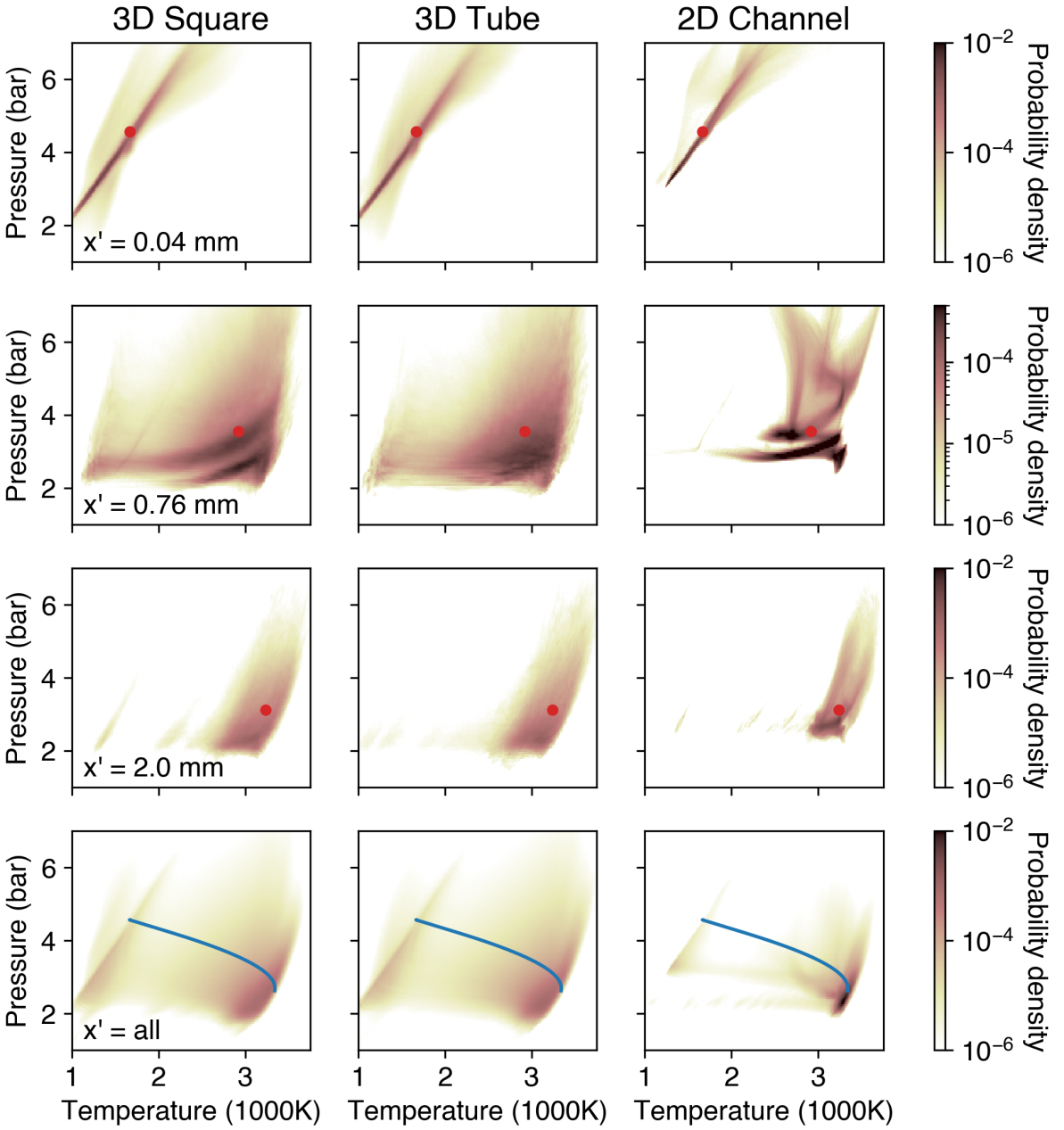

Figure 2: 2D histogram plots (pressure and temperature) showing thermodynamic state statistical distribution of grid cells in simulations. First row is for grid cells immediately behind shock wave ($x' = 0.04$ mm), second for grid cells behind the induction zone ($x' = 0.76$ mm), third for grid cells behind reaction zone ($x' = 2$ mm) and forth for all post-shock grid cells. First column is for 3D square channel, second for 3D tube, and third for 2D channel. Superimposed is ZND solution (red dot for single x'-position or blue line for all x'). Colorbar applies to all horizontal figures.

confining geometry can lead to substantial changes in cellular structure, this does not necessarily lead to changes in the average structure or propagation velocity. The 2D simulation profile shows somewhat higher temperatures and pressures as compared to the 3D simulation. Interestingly, despite the very small velocity deficit (≈3% for 3D cases, and 0.3% for 2D case), the mean temperatures and pressures are substantially reduced as compared to the ZND profile. This could be attributed in part to wall losses

in the post-reaction zone.

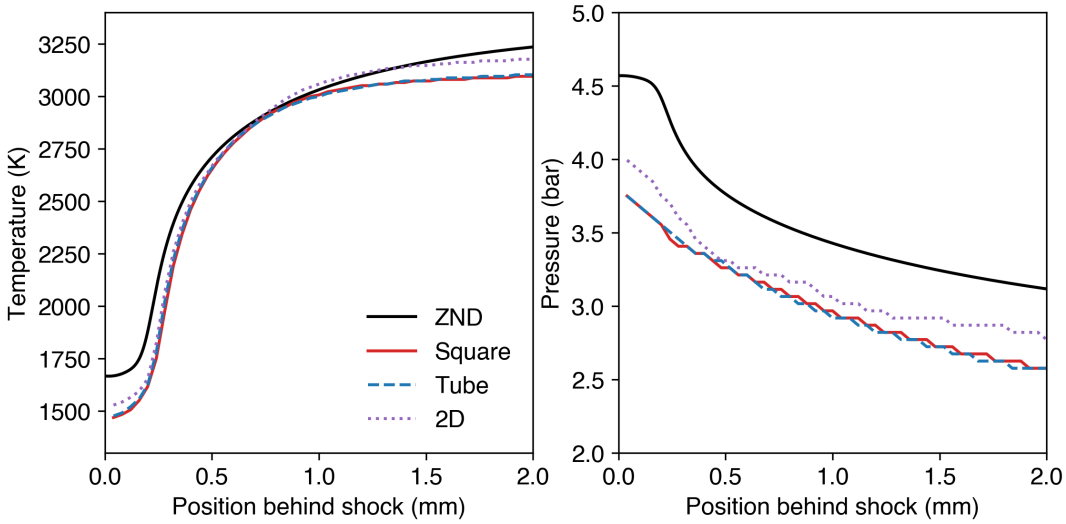

Figure 3: ZND solution and Reynolds-averaged mean temperature and pressure profiles for 3D square (red line), 3D tube (blue dashed line), and 2D channel (purple dotted line) simulations. Legend applies to both plots.

4 Conclusions

By analyzing the statistical distribution of thermodynamic states (temperature and pressure) present in 2D and 3D simulations of varying confining geometries, the following conclusions are made for the present mixture conditions (stoichiometric hydrogen-oxygen doped with 3000 PPMv ozone):

- Differences in 3D detonation structure manifest in differences in the statistical distribution of thermodynamic states in the post-induction zone.
- Despite the differences in cell structure and post-induction zone statistics for the 3D square channel and round tube simulations, the mean structure is qualitatively similar between these geometries. This result suggests that the details of the cellular structure do not appreciably dictate the mean propagation characteristics.
- 3D simulations exhibit a substantially wider set of thermodynamic states as compared to 2D simulations. This has implications for the modeling of non-linear physics such as finite-rate kinetics and post-shock vibrational relaxation. Care should be taken when interpreting 2D simulation results given that these simulations only contain a subset of the conditions expected in real detonations.

References

[1] L. Shi, H. Shen, P. Zhang, D. Zhang, and C. Wen, "Assessment of vibrational non-equilibrium effect on detonation cell size," *Combustion Science and Technology*, vol. 189, no. 5, pp. 841–853, 2017.

[2] F. Haloua, M. Brouillette, V. Lienhart, and G. Dupré, "Characteristics of unstable detonations near extinction limits," *Combustion and Flame*, vol. 122, no. 4, pp. 422–438, 2000.

[3] X. Shi, J. Crane, and H. Wang, "Detonation and its limit in small tubes with ozone sensitization," *Proceedings of the Combustion Institute*, vol. 38, no. 3, pp. 3547–3554, 2021.

[4] J. Crane, J. T. Lipkowicz, X. Shi, I. Wlokas, A. M. Kempf, and H. Wang, "Three-dimensional detonation structure and its response to confinement," *Proceedings of the Combustion Institute*, 2022.

[5] M. I. Radulescu, G. J. Sharpe, C. K. Law, and J. H. Lee, "The hydrodynamic structure of unstable cellular detonations," *Journal of Fluid Mechanics*, vol. 580, pp. 31–81, 2007.

[6] M. D. Frederick, R. M. Gejji, J. E. Shepherd, and C. D. Slabaugh, "Statistical analysis of detonation wave structure," *Proceedings of the Combustion Institute*, 2022.

[7] J. Crane, X. Shi, A. V. Singh, Y. Tao, and H. Wang, "Isolating the effect of induction length on detonation structure: Hydrogen–oxygen detonation promoted by ozone," *Combustion and Flame*, vol. 200, pp. 44–52, 2019.

[8] M. Rieth, F. Proch, M. Rabaçal, B. M. Franchetti, F. C. Marincola, and A. M. Kempf, "Flamelet LES of a semi-industrial pulverized coal furnace," *Combustion and Flame*, vol. 173, pp. 39–56, 2016.

[9] J. T. Lipkowicz, I. Wlokas, and A. M. Kempf, "Analysis of mild ignition in a shock tube using a highly resolved 3D-LES and high-order shock-capturing schemes," *Shock Waves*, vol. 29, no. 4, pp. 511–521, 2019.

[10] G. P. Smith, Y. Tao, and H. Wang, "Foundational fuel chemistry model version 1.0 (FFCM-1), http://nanoenergy.stanford.edu/ffcm1," 2016.

[11] Y. Tao, G. P. Smith, and H. Wang, "Critical kinetic uncertainties in modeling hydrogen/carbon monoxide, methane, methanol, formaldehyde, and ethylene combustion," *Combustion and Flame*, vol. 195, pp. 18–29, 2018.

[12] H. Zhao, X. Yang, and Y. Ju, "Kinetic studies of ozone assisted low temperature oxidation of dimethyl ether in a flow reactor using molecular-beam mass spectrometry," *Combustion and Flame*, vol. 173, pp. 187–194, 2016.

[13] A. R. Kasimov and D. S. Stewart, "On the dynamics of self-sustained one-dimensional detonations: A numerical study in the shock-attached frame," *Physics of Fluids*, vol. 16, no. 10, pp. 3566–3578, 2004.